Energy, Volume 182, Issue September, 2019, pp. 641-655
DOI:10.1016/j.energy.2019.05.180

Thermodynamic analysis of nutating disc engine topping cycles for aero-engine applications

Joshua Sebastiampillai[a*], Andrew Martin Rolt[a], Florian Jacob[a], Devaiah Nalianda[a], Vishal Sethi[a]

[a] Centre for Propulsion Engineering, Cranfield University, College Road, Cranfield, Bedfordshire MK43 0AL, UK;
[b] Empresarios Agrupados Internacional, C/Magallanes, Madrid 28015, Spain; pce@empre.es

* Corresponding author. Email: j.sebastiampillai@cranfield.ac.uk; Tel. +44-1234-755-414

Abstract

Within the next thirty years the evolutionary approach to aero engine development will struggle to keep abreast with increasingly stringent environmental targets. Therefore radical approaches to aero-engine development in terms of energy savings need to be considered. One particular concept involves the inclusion of a pressure-rise combustion system, within the architecture of an aero-engine, to provide additional shaft power. The nutating disc engine concept is a strong contender due to its power density. The feasibility of the nutating disc engine has been previously investigated for unmanned vehicle applications. However, this paper investigates the performance benefits of incorporating a nutating disc core in a larger geared open rotor engine for a potential entry in to service in 2050. In addition, a methodology is presented to estimate the size and weight of the nutating disc core. This methodology is pivotal in determining the overall performance of the novel aero-engine cycle. The outcome of this study predicts a potential 9.4% fuel burn benefit, over a state of the art geared open rotor in the year 2050. In addition, the sensitivity of the nutating disc design variables was explored. This showcases a pessimistic design and an optimistic design, showing the range of possible fuel burn benefits compared to a comparable year-2000 aircraft mission.

Highlights

- The nutating disc engine, is a power-dense internal combustion engine that claims high thermal efficiency.
- This study investigates the benefit derived from integrating a Dual-cycle (Otto and Diesel) within a Brayton cycle.
- A methodology to predict the size and weight of the nutating disc engine is presented. This is essential to determine aircraft mission level fuel burn benefits/penalties
- When the nutating disc engine is integrated into the architecture of a year 2050 geared open rotor and aircraft, the potential fuel-burn benefit is 9.4% relative to a year 2050 baseline aircraft.

Keywords: Nutating disc engine, ULTIMATE, combined cycle, fuel burn, geared open rotor.

Glossary

Property	***Units***	***Description***
#ND	*(-)*	*number of nutating disc cores*
a	*(m/s)*	*speed of sound*
$A_{i/e\|\|plenum}$	*(m^2)*	*inlet/ exit area of either the inlet or exhaust plenum*
BnBf	*(-)*	*Number of propeller blades for the front propeller array*
BnBr	*(-)*	*Number of propeller blades for the rear propeller array*
$CA_{combustion}$	*(deg.)*	*Crank angle per shaft revolution for combustion*
CR	*(-)*	*cruise condition*
DE	*(m)*	*height of the ND combustion chamber*
EOR	*(-)*	*End of Runway*
FB2000	*(%)*	*Fuel burn benefit/penalty relative to a comparable year 2000 mission*
FB2050	*(%)*	*Fuel burn benefit/penalty relative to a comparable year 2050 mission*

Fn	*(kN)*	*net thrust*
$f_{pl,23}$	*(-)*	*Total pressure loss between the nutating disc compressor and accumulator*
$f_{pl,34}$	*(-)*	*Total pressure loss between the nutating disc accumulator and pre-combustion chamber*
$f_{ql,cy}$	*(-)*	*heat loss ratio through the pre-combustor walls*
HT	*(-)*	*hub to tip ratio*
$IPC\ PR$	*(-)*	*intermediate pressure compressor pressure ratio*
$IPT\ PR$	*(-)*	*intermediate pressure turbine pressure ratio*
k	*(-)*	*number of power cycle per shaft revolution of the nutating disc engine*
l_f	*(-)*	*wedge radius to tip radius of nutating compressor disc*
$L_{o,duct}$	*(m)*	*axial length of the duct upstream of the inlet plenum*
L_{HV}	*(MJ/kg)*	*lower heating value*
li_{max}	*(m)*	*maximum length of the runners/manifolds that connect the plenum to the nutating disc cores*
$LPT\ PR$	*(-)*	*Low pressure turbine pressure ratio*
$ND\ r_{23}$	*(-)*	*nutating disc engine expansion ratio from the compression chamber to the accumulator*
$ND\ r_{34}$	*(-)*	*nutating disc engine expansion ratio from the accumulator to the pre-combustion chamber*
$Nmech$	*(rpm)*	*Turbomachinery rotational speed*
Ns	*(rps)*	*operational speed*
OPR	*(-)*	*overall pressure ratio*
p_{xx}	*(-)*	*Coefficients in swept volume estimation*
r_{12}	*(-)*	*volumetric compression ratio*
r_{67}	*(-)*	*Volumetric expansion ratio*
r_{71}	*(-)*	*Overall volumetric ratio, if above unity indicates that expander disc is bigger than the compressor disc in a dual disc configuration*
r_h	*(m)*	*hub radius*
r_t	*(m)*	*tip radius*
SFC	*(g/kNs)*	*specific fuel consumption*
$T_{01\text{-}07}$	*(K)*	*total temperatures at stations 1 through to 7 in the nutating disc engine*
T_{06mx}	*(K)*	*maximum total temperature at the end of constant pressure combustion*
$V_{1,2}$	*(m^3)*	*volume definitions used in the definition of the swept nutating disc engine volume*
V_{An}	*(m^3)*	*revolved area of triangular section of the nutating disc*
V_{Ao}	*(m^3)*	*revolved area of circular section of the nutating disc*
V_{casing}	*(m^3)*	*nutating disc casing volume*
$V_{disp\_disc1,2}$	*(m^3)*	*displaced volume in either compressor or expander disc*
V_{ND}	*(m^3)*	*volume of nutating disc*
V_{plenum}	*(m^3)*	*volume of toroidal plenum*
V_{wedge}	*(m^3)*	*volume estimate of the nutating disc wedge*
V_{sw}	*(m^3)*	*swept volume*
W	*(kg/s)*	*Mass flow*
$\dot{W}_{56}$	*(kW)*	*net work done during the constant pressure combustion process in the nutating disc engine*
$\dot{W}_{67}$	*(kW)*	*net work done during the expansion process in the nutating disc engine*
$\dot{W}_c$	*(kW)*	*net work needed during the compression process in the nutating disc engine*
$\dot{W}_{net}$	*(kW)*	*net shaft work produced by the ND engine*
α	*(deg)*	*angle of nutation*
η_{poly}	*(-)*	*Polytropic efficiency of IPC, IPT or LPT*

$\eta_{s,c}$	*(-)*	*isentropic compression efficiency*
$\eta_{s,e}$	*(-)*	*isentropic expansion efficiency*
η_{bu}	*(-)*	*burner efficiency*
η_{me}	*(-)*	*mechanical efficiency*
η_{TH}	*(-)*	*Thermal efficeincy*
η_v	*(-)*	*volumetric efficiency*
θ_1	*(-)*	*maximum temperature change ratio*
θ_2	*(-)*	*average temperature change ratio*
ρ_i	*(kg/m^3)*	*inlet density*
ψ	*(deg)*	*semi-wedge angle*
ω	*(rad/s)*	*rotational speed*
ϕ	*(deg)*	*crank angle per shaft revolution*
$\phi_{i,e}$	*(deg)*	*crank angle per shaft revolution at the beginning or end of a process*

1 Introduction

Demand in the aviation sector is projected to grow at an annual rate of 4.1% within the next 20 years [1]. These projections coupled with emissions projections for 2050 call for action within the civil aviation turbofan sector to significantly reduce greenhouse gas emissions by 2050 [2]. The pace of innovation within the sector, primarily due to tight certification legislation and high capital investments, means a concept can take roughly 15 years from the preliminary design phase to entry into service [3]. In order to address these issues, the Advisory Council for Aviation Research and Innovation in Europe (ACARE) has issued a strategic research and innovation agenda (SRIA). The SRIA sets five major challenges for the aviation sector by the year 2050. One of the more pressing challenges is the third SRIA challenge. This challenge targets reducing mission-level energy consumption and CO_2 emission levels by 75% by the year 2050, when compared to year-2000 baseline energy consumption levels.

Based on projections of historic rates of fuel-burn reduction using evolutionary approaches of aero-engine development, it is postulated that the aviation sector will not be able to meet the 75% energy consumption reduction target by the year 2050. Hence, a step decrease in fuel burn is required. Prior to determining which path this study will employ to address the SRIA 2050 targets, an overall perspective is provided for the potential magnitude of fuel-burn savings stemming from flight path optimization, aircraft improvements and engine improvements, respectively. According to Jensen et al., optimization of flight paths and speeds lead to potential fuel-burn reductions of 1.75% to 1.96% for short haul missions [4]. The work conducted by Nickol et al. indicates that the potential fuel-burn benefits for advanced tube and wing aircraft concepts, from introducing technologies that reduce drag and weight, amounts to roughly 20% for short haul missions [5]. From the same work, it was shown that the advances in engine technology could potentially amount to roughly 19% in fuel-burn savings [5]. It can be surmised that the relative magnitude of fuel-burn savings imparted by the engine alone can outweigh the potential fuel-burn benefits derived from the individual component technologies that contribute to fuel burn in an advanced tube and wing aircraft [5]. Consequently, priority should be given to technologies that increase the overall efficiency of the gas turbine.

In order to increase aero engine thermal efficiency, manufacturers have historically increased the turbine entry temperatures (TET), overall pressure ratios (OPR) and component efficiencies of high bypass ratio turbofans [6,7]. Theoretically this allows the cycle to operate at higher overall efficiency, but the potential for higher thermal efficiency from increasing TET is reaching its apogee, as TET is limited by cooling requirements and the material operating temperatures of the high pressure (HP) turbine. The combustor flame temperature may also be limited to meet legislated NOx limits [8]. Furthermore, increasing OPR leads to smaller blade-heights in the last stages of the HP compressor, tending to reduce its component efficiency. Consequently, a step beyond the current trend of increasing TET and OPR is required in order to significantly improve thermal efficiency. A promising option is to attack the ‘combustor’ losses in a standard Brayton-cycle-based gas-turbine. This study

looks a novel way in which this might be achieved in an open rotor engine for short-range missions in the year-2050 (Y2050) timeframe [9].

Currently the combustion process across a standard annular combustion chamber includes a total pressure drop. This characteristic contributes to overall combustor losses and costs several percentage points of thermal efficiency, but it is not the biggest source of combustor loss[10]. Thermodynamically, the current gas turbine combustion process is described as constant pressure or isobaric, but entropy generation can be reduced by moving closer towards a constant volume, or isochoric combustion process. Fig. ***1*** shows the thermodynamic benefit derived from an isochoric combustion process, when compared to an isobaric combustion process, in terms of the entropy generated for a fixed combustion temperature [11]. The benefit of an isochoric process stems from the 1st law of thermodynamics, as the heat added to a fixed control volume increases the specific enthalpy of the system and raises its pressure with a small increase in entropy. Conversely, in an adiabatic isobaric combustion process the heat added, as well as raising temperature, does work by expanding the flow at constant pressure, with a greater increase in entropy. Practically, the benefits of the isochoric combustion process can be seen when comparing the overall efficiency of a good internal combustion engine (45%) versus a standard heavy duty land-based gas turbine (37-40%) [12]. Consequently, it should pay to adopt constant volume combustion technology in order to increase thermal efficiency.

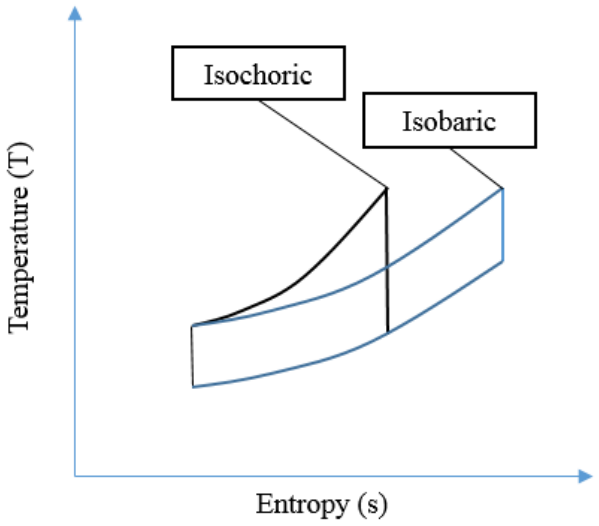

Fig. 1: Theoretical benefit derived from an isochoric combustion process as opposed to an isobaric combustion process. [**Colour not necessary**].

Several attempts were made circa 1950 to incorporate constant volume combustion technologies into the architecture of gas turbine aero engines, but without any commercial success. However, a relatively new candidate pressure rise combustion machine concept might be more competitive in aerospace applications. This engine concept is referred to as the Nutating Disc (ND) engine. The operation of the ND engine, as well as the definition of its thermodynamic performance, is described by Korakianitis et al. [13]

The ND engine (Fig. ***2***(a)) uses separate chambers for compression, combustion and expansion processes, in comparison to most piston engines, where all the processes take place within the same chamber. Its operation is more comparable to that of a gas turbine since the thermodynamic processes are carried out in separate components [13]. A unique feature of the ND engine is its ability to use both sides of its working disc during a full shaft revolution. This design feature contributes to its potential for high power density. Fig. ***2***(a) illustrates the components of a naturally-aspirated single-disc nutating-disc engine. The layout comprises an inlet, compression chamber, accumulator, combustion chamber, expansion chamber and exhaust manifold, with the nutating disc mounted inside the compressor and expander chambers [13]. The disc itself is basically bi-conical with a spherical hub. Fig. **2**(b) shows that air enters the compression chamber through an 'elbow-duct'. The air is subsequently trapped and compressed by the nutating motion of the disc and stored in an

accumulation chamber. The compressed air then passes into the combustion chamber through a valve and is mixed with fuel and ignited, either by a spark-plug, or by compression ignition. Constant-volume combustion occurs in the combustion chamber, followed by roughly constant-pressure combustion through a portion of the expansion chamber. The latter primarily due to the short residence time in the combustion or 'pre-combustion' chamber. Finally, the hot gases expand through the rest of the expansion chamber and exit through exhaust-valves or exhaust-ports to the exhaust manifold. The excess power is transmitted by a z-shaft, which converts the nutating motion into a rotating motion when the z-shaft is coupled to a further shaft. These processes are applicable to both single-disc and dual-disc nutating disc engine configurations.

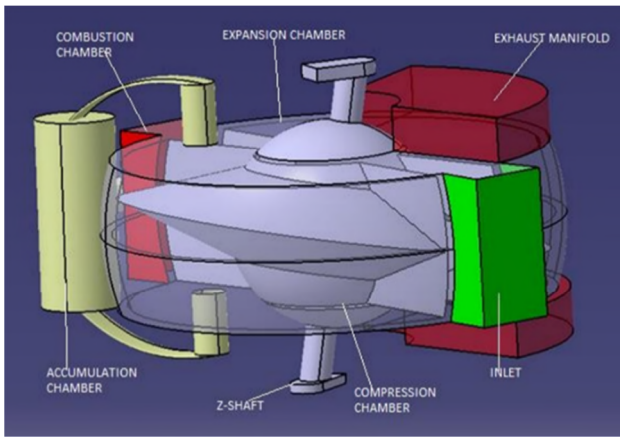

Fig. 2(a): Single-disc ND engine [**Colour necessary**].

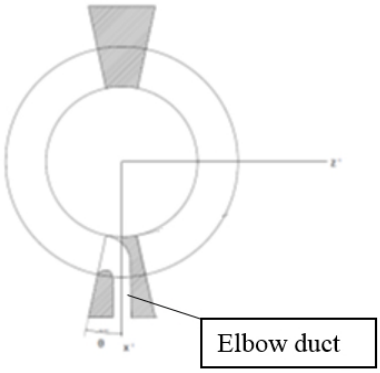

Fig. 2(b): Top-down view of a single ND engine indicating the elbow duct [**Colour not necessary**].

The main drawback of the single-disc ND-engine configuration is that its structure is subject to very uneven thermal loading during operation. This is likely to reduce life particularly considering seal-efficiency deterioration. To alleviate this inherent issue, a two-disc arrangement is proposed, as shown in Fig. ***3***. In this case, separate discs are dedicated to the compression and expansion processes, and the discs consequently have more-symmetrical thermal loadings. Optionally, the two discs may have different sizes in order to optimise the overall design.

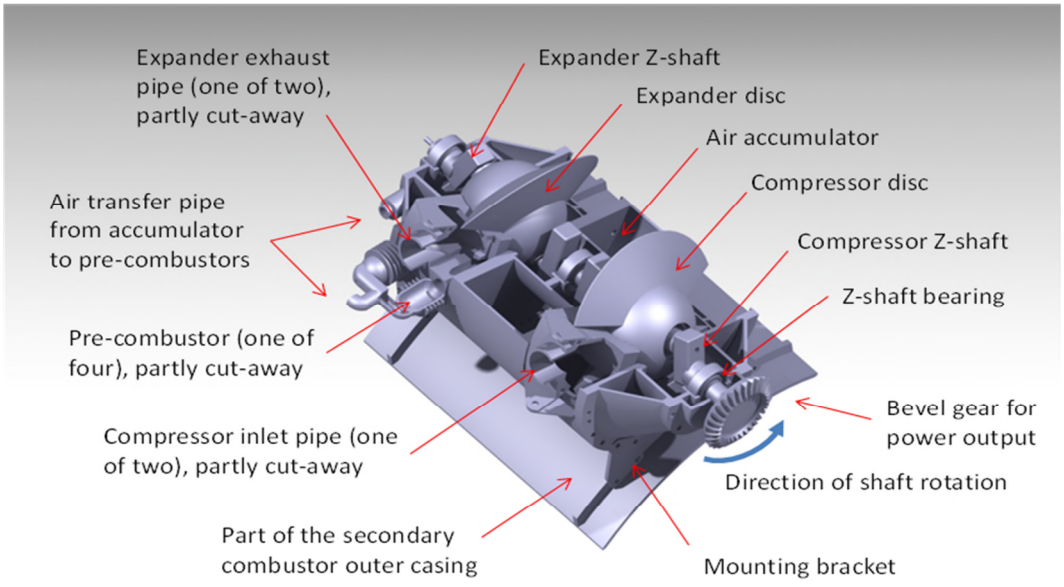

Fig. 3: Cut-away representation of a dual-disc nutating-disc engine [**Colour necessary**].

Korakianitis et al. claim the operational benefits offered by the ND engine include significantly lower bearing loads relative to piston engines, a relatively smooth torque curve to ensure high

mechanical transmission efficiency, and a high power to volume ratio [13]. These features of the ND engine make it an attractive potential candidate for an aero-engine. The smooth torque curve reflects the almost-steady inlet and exhaust flows. This particular feature makes the aerodynamic coupling between the continuous-flow turbomachinery and the discontinuous-flow ND engine more efficient. When considering technology enablers for aero engines, high power to weight ratio is at a premium and hence the ND engine could be a viable candidate pressure-rise combustor technology.

To date, the state-of-the-art work reported on the ND engine is that performed by Korakianitis et al. In addition to having presented the thermodynamic model of the ND engine [13], the performance of a multi-disc ND engine configuration and the potential of using single-disc ND engines for unmanned aerospace vehicle (UAV) applications have been presented [14][15]. The conclusions drawn from [14] claim that the ND engine in the dual-disc engine configuration offers a significant degree of design flexibility in terms of providing variable-compression ratio and having an expansion ratio greater than the compression ratio. In addition, it is claimed that the optimal power range where the specific power of the normally-aspirated ND engine is more favourable than a gas turbine is between 2 and 500kW[14]. Furthermore it is claimed that in that power range, the ND-engine is also a viable competitor with piston engines [15]. However, to the authors' knowledge, there are no published assessments of the performance of a ND-topped combined-cycle aero-engine, nor a methodology to predict the size and capacity of such a ND engine.

Thus the primary focus of this paper is to present a methodology to predict the size of the ND engine and estimate the performance of a ND-core-topped aero-engine cycle for possible entry into service by 2050. Since the technology readiness level (TRL) of the ND-engine is low, compared to alternative pressure-rise combustion technologies, its integration with a reference 2050 short-range engine architecture will be considered. Fig. ***4*** indicates the arrangement of a ND engine core within the architecture of a geared open rotor engine (GOR). The core comprises several parallel-flow double-nutating-disc modules, which are circumferentially distributed around the centre line of the engine.

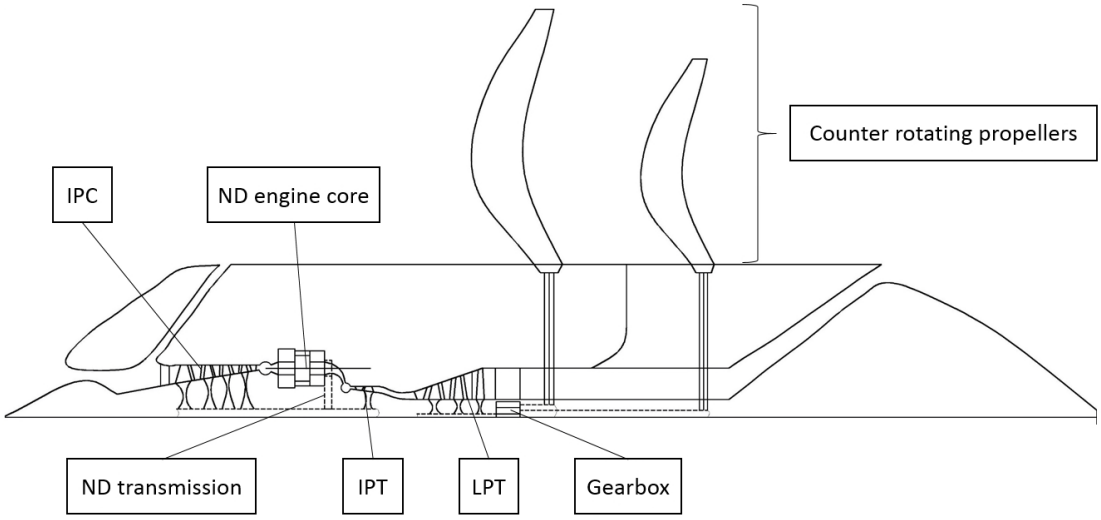

Fig. 4*: Pusher GOR 2050 configuration with nutating disc engine core* [**Colour not necessary**].

2 Methodology

The simulations necessary for predicting the performance and size of a ND engine topping cycle, were conducted using the software called "Propulsion Object Oriented Simulation Software" (PROOSIS 3.6.14, Empresarios Agrupados Internacional, Madrid, Spain) [16]. The TURBO library version 3.2.3, present in the PROOSIS software package, contains quasi-1D representations of turbomachinery components via representative component maps [17]. Although the pre-set tools in the TURBO library are adequate to assess the performance of standard gas turbine architectures, they do not suffice for estimating the performance of the ND-core-topped composite cycle. Hence, the new components that have been constructed to estimate the performance and weight of the engine configuration are the:

- Quasi-1D nutating disc component
- Interconnecting Plenum component

The impact of the engine weight and steady-state performance on mission fuel-burn, throughout a potential flight envelope, must be considered in order to benchmark the engine configuration against the 2050 SRIA targets. Therefore, a methodology to predict the weight of the engine configuration, as well as a method to predict the relative fuel-burn benefits compared to a reference engine case, are presented. The reference engine configuration used for benchmarking the benefits derived by the ND-engine configuration is the Y2050 reference geared open rotor. **Table *1***, indicates the performance of this reference engine. The quoted figures in **Table *1*** are an outcome of the authors' assessment of the performance of a reference year 2050 geared open rotor made in the Horizon 2020 ULTIMATE project [18]. The weight of the reference engine is 3197 kg, including the weight of the gearbox, propeller and fuel systems. Finally, the predicted fuel-burn benefit of the reference geared open rotor powered aircraft, when compared to a year-2000 (Y2000) short-range aircraft with turbofan engines, is a reduction of 59.5%.

Table 1*: Performance of year 2050 reference geared open rotor configuration*

Parameter	***Top of Climb***	***Cruise***	***End of runway***
Mach number(-)	*0.73*	*0.71*	*0.20*
Altitude (m)	*10688*	*11278*	*0*
Net Thrust (kN)	*17.34*	*13.85*	*78.95*
OPR(-)	*41.1*	*36.8*	*33.4*
TET(K)	*1750*	*1628*	*1950*
EGT(K)	*726*	*672*	*910*
SFC(g/kN.s)	*10.75*	*10.41*	*6.44*

2.1 Nutating disc performance model

The thermodynamic cycle that best describes a nutating disc engine is akin to a 'dual cycle', that is part Otto cycle and part Diesel cycle [13]. Fig. ***5*** shows a P-V diagram that represents the thermodynamic processes within a nutating disc engine, irrespective of its configuration (single-disc or multi-disc).

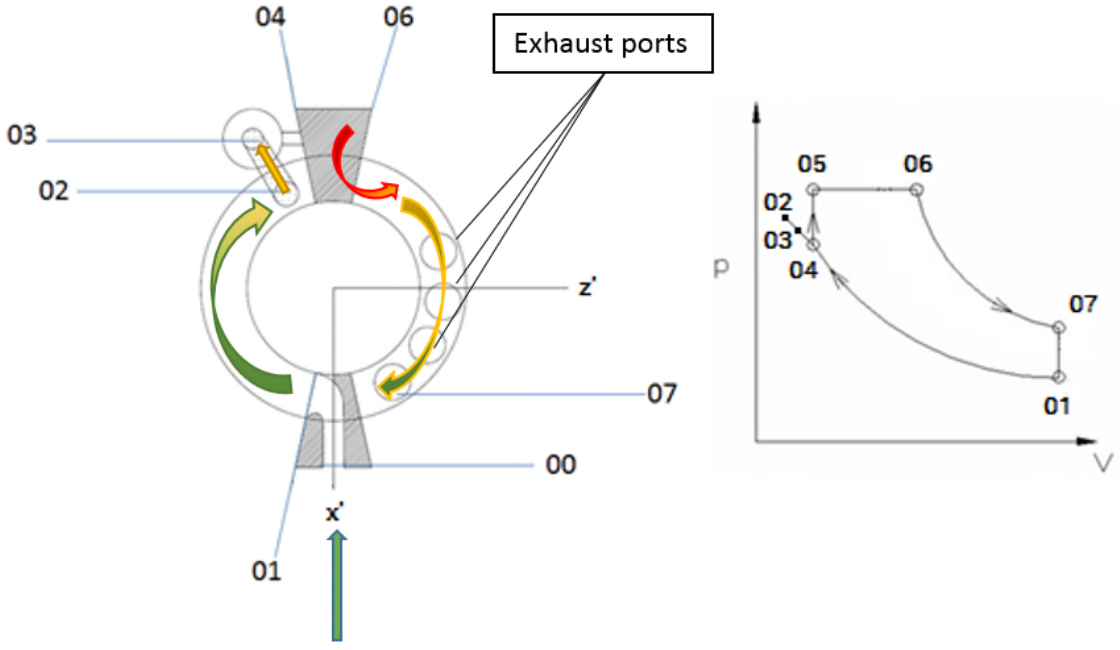

Fig. 5*: Thermodynamic stations mapped to the geometry of a naturally-aspirated ND engine* [**Colour necessary**].

Figure 5 also shows a top-down view of a single-nutating-disc engine configuration, in order to map the thermodynamic processes to the subcomponents of the engine. The thermodynamic processes of the cycle can be described as follows [15]:

- Process 01-02: adiabatic isentropic compression of the working fluid,
- Processes 02-04: adiabatic expansion of the fluid from the end of the compression process through the accumulator and into the combustion chamber,
- Processes 04-06: the constant volume combustion and constant pressure combustion (either spark or compression ignited),
- Process 06-07: adiabatic expansion of the combustion products through to the exhaust ports.

The thermodynamic processes occur on both sides of the disc 180° out-of-phase, and overlap each other by shaft-rotation angles of about 90°. This means that two complete cycles are achieved per shaft revolution [15].

The methodology proposed by Korakianitis et al., adequately describes the performance of a naturally-aspirated nutating-disc engine. However, a methodology to incorporate the size of a single disc or dual-disc nutating-disc engine is necessary to provide a better estimation of performance and weight and the potential for integrating the technology within the architecture of a gas turbine engine. Figure 6 gives an overview of the independent geometric design variables that influence the performance of the nutating-disc engine, as well as the design variables that determine the overall performance of the nutating disc engine [13].

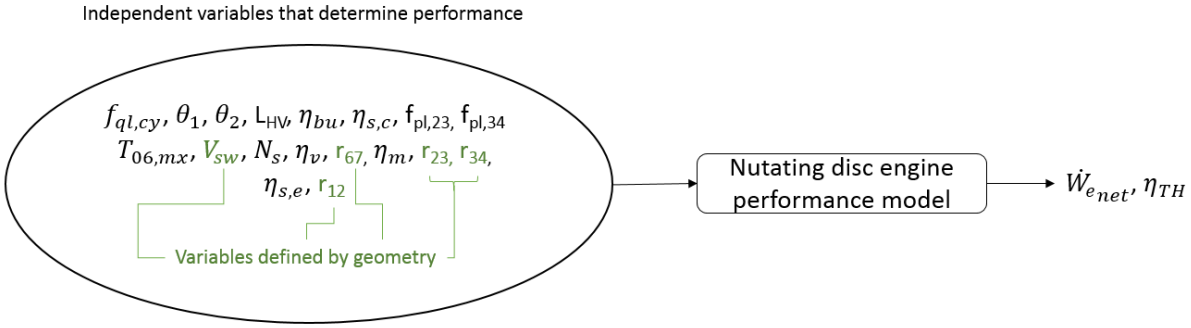

Fig. 6*:* Overview of design variables that are used to determine nutating disc engine performance [**Colour not necessary**].

2.2 Swept volume estimation of a dual-nutating-disc engine configuration

The swept volume (V_{sw}) of the nutating-disc engine can be determined by defining the tip radius (r_t), hub radius (r_h), angle of nutation (α) and the wedge radius (r_l) of each disc, as shown in Figure 7.

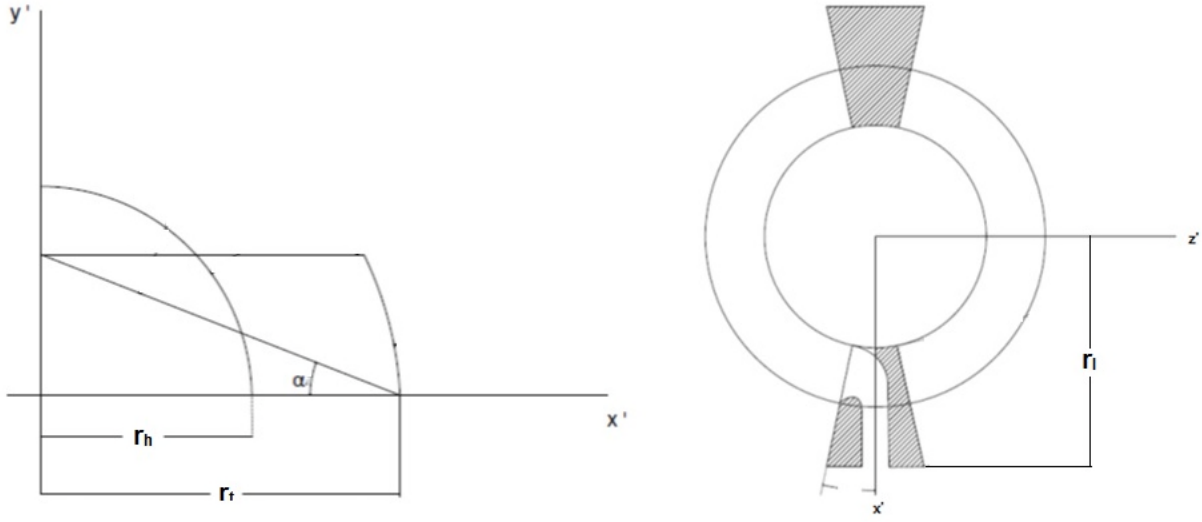

Fig. 7*:* Definition of the variables that determine the size of a single disc [**Colour not necessary**].

2.2.1 Casing volume estimation

The volume enclosed by the casing of a single nutating disc is expressed as a function of the tip radius and the angle of nutation. It is assumed that there is no clearance between the net nutating disc internal volume and the casing. Figure 8 depicts what is meant by the casing volume. The casing volume is defined in Equation (1), where the angle of nutation is expressed in radians.

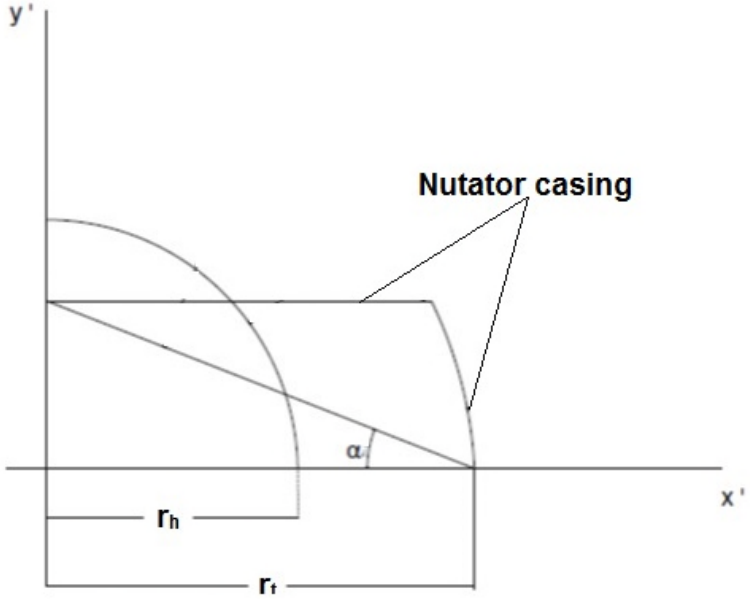

Fig. 8*: Nutating disc casing definition* [**Colour not necessary**].

$$V_{casing} = 2\pi[r_t^3 \sin(\alpha) - \frac{[r_t \sin(\alpha)]^3}{3}] \quad (1)$$

2.2.2 Wedge volume estimation

Two wedges are placed in each of the compressor and expander disc chambers, diametrically opposite to each other. These admit air through 'elbow-ducts' into the compressor disc chamber, and exhaust the products of combustion from the expander disc chamber. The volume of the wedge can be expressed as a function of the hub to tip ratio of the nutating disc (HT), the wedge semi-angle (ψ) and the wedge radius to disc tip radius ratio (l_f). Figure 9 shows the definition of the arrangement of the wedge. The wedge's gross volume is estimated by sweeping its profile through its total wedge-angle. The volume of the wedge that is enclosed within the casing of the disc is calculated by Equation (6).

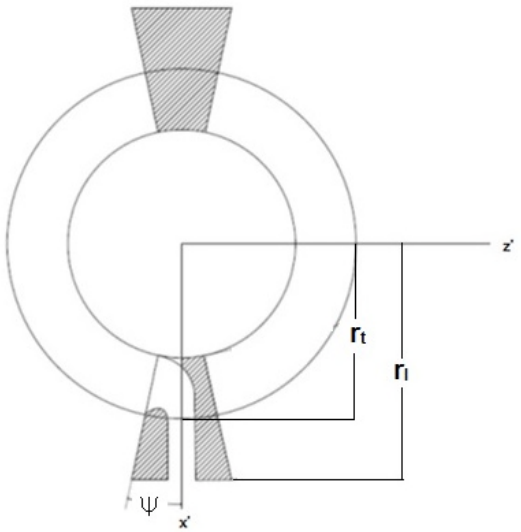

Fig. 9*:* Definition of wedge parameters [**Colour not necessary**].

$$HT = \frac{r_h}{r_t} \tag{2}$$

$$l_f = \frac{\mathrm{r_l}}{r_t} \tag{3}$$

$$\psi = \mathrm{atan}\left(\frac{r_t - r_h}{2 r_t l_f}\right)\left(\frac{180}{\pi}\right) \tag{4}$$

$$\psi = \mathrm{atan}\left(\frac{r_t - r_h}{2 r_t l_f}\right)\left(\frac{180}{\pi}\right) \tag{5}$$

$$V_{wedge} = \frac{2\pi\psi}{180}\left[\int_{-r_t \sin(\alpha)}^{r_t \sin(\alpha)} r_t^2 - y'^2 dy' - \int_{-r_t \sin(\alpha)}^{r_t \sin(\alpha)} r_h^2 - y'^2 dy'\right. \tag{6}$$

2.2.2 Disc volume estimation

The nutating disc itself is housed within the casing at an orientation defined by the angle of nutation and the crank angle. In order to estimate the volume that the nutating disc occupies within the casing, the areas A_O and A_N are revolved around the y' axis, as indicated in Figure 10.

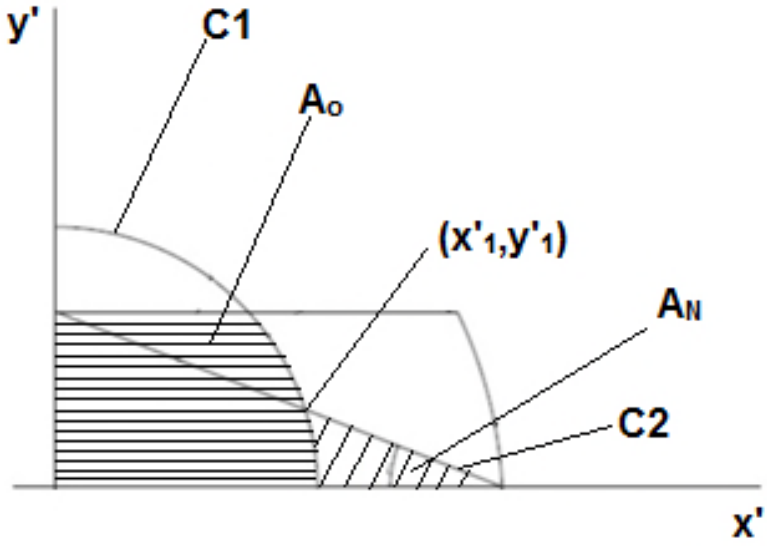

Fig. 10*:* Definition of the nutating disc areas that are revolved around the y′ axis [**Colour not necessary**].

The volume swept by A_N is defined by Equations (7) to (9), where the upper limit in the volume of revolution integral (y'_1) is defined as a function of the disc-tip radius, hub to tip ratio and angle of nutation. The upper limit (y'_1) is defined parametrically by finding the spatial coordinates where curves C1 and C2 intersect, as shown in Figure 10.

$$V_{A_n} = V_1 - V_2 \tag{7}$$

$$V_1 = \pi \int_0^{y'_1} r_t^2 - 2 r_t y' \tan(\alpha)^{-1} + y'^2 (\tan(\alpha))^{-2} dy' \tag{8}$$

$$V_2 = \pi \int_0^{y'_1} r_h^2 - y'^2 dy' \tag{9}$$

The volume of the solid that is defined when A_O is revolved about the y′ axis is indicated in Equation (10), where the upper-limit of the integral is defined by the height of the casing. Consequently, the total volume occupied by the nutating disc in the casing is given by Equation (11).

$$V_{A_o} = \pi \int_0^{r_t \sin(\alpha)} r_h^2 - y'^2 dy' \tag{10}$$

$$V_{ND} = V_{A_N} + V_{A_o} \quad (11)$$

Therefore the volume displaced in a single nutating-disc chamber can be estimated by appropriate accounting of the internal volumes as shown in Equation (12).

$$V_{disp_{disc1}} = V_{casing} - 2(V_{ND} + V_{wedge}) \quad (12)$$

In order to account for the volume displaced by the expander nutating-disc compartment, in a dual-disc arrangement, the overall relative volumetric expansion ratio (r_{71}) is defined in Equation (13) so that the diameter of the expander disc is calculated [14]. Note this assumes the wedge angles, disc hub to tip radius ratios and angles of nutation are equal.

$$r_{71} = \left(\frac{r_{disc1}}{r_{disc2}}\right)^3 \quad (13)$$

Consequently if Equations (1) to (12) are used for the expander disc, the corresponding volume displaced by the expander disc ($V_{disp_{disc2}}$) can be determined. Therefore the volume displaced by a dual-disc nutating-engine configuration is estimated by Equation (14). Furthermore, the swept volume estimated for one shaft revolution is expressed as a function of the number of power cycles per shaft revolution (k).

$$V_{disp} = V_{disp_{disc1}} + V_{disp_{disc2}} \quad (14)$$

$$V_{sw} = \frac{V_{disp}}{k} \quad (15)$$

2.3 Volumetric compression ratio estimation

The volumetric compression ratio can be expressed as a function of the tip radius, hub to tip ratio, angle of nutation and the crank angle per shaft revolution (ϕ). In order to account for the variation in the disc position within the casing, as a function of the crank angle, the tip and hub radii need to be projected from the dynamic frame of reference to a static frame of reference, as shown in Figure 11.

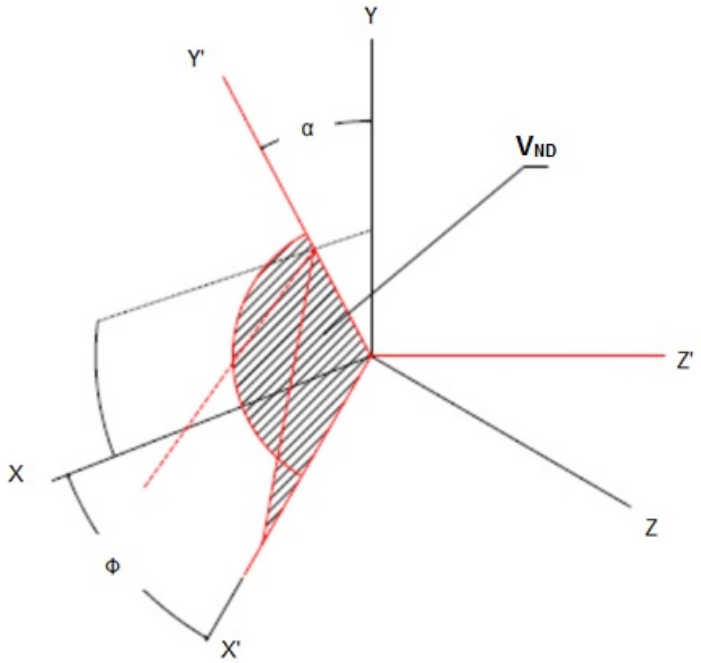

Fig. 11: Projection of the dynamic frame of reference on to the static frame of reference [**Colour necessary**].

The crank angle per shaft revolution is expressed as a function of the rotational speed (ω) in radians per second, and time (t) in seconds. Consequently, the tip and hub radii are transformed from the dynamic frame of reference to the static frame of reference.

$$\phi = \omega t \quad (16)$$

$$r_{t(\phi)} = r_t \cos(\phi)\cos(\alpha)\,; \;\; r_{h(\phi)} = r_h \cos(\phi)\cos(\alpha) \quad (17)$$

To make a representative approximation of the volumetric compression ratio, the displaced volume is calculated at a crank angle corresponding to the beginning of compression process (ϕ_i) and again at the end of the compression process (ϕ_e). Figure 12 shows the two instances where the displaced volume should be calculated.

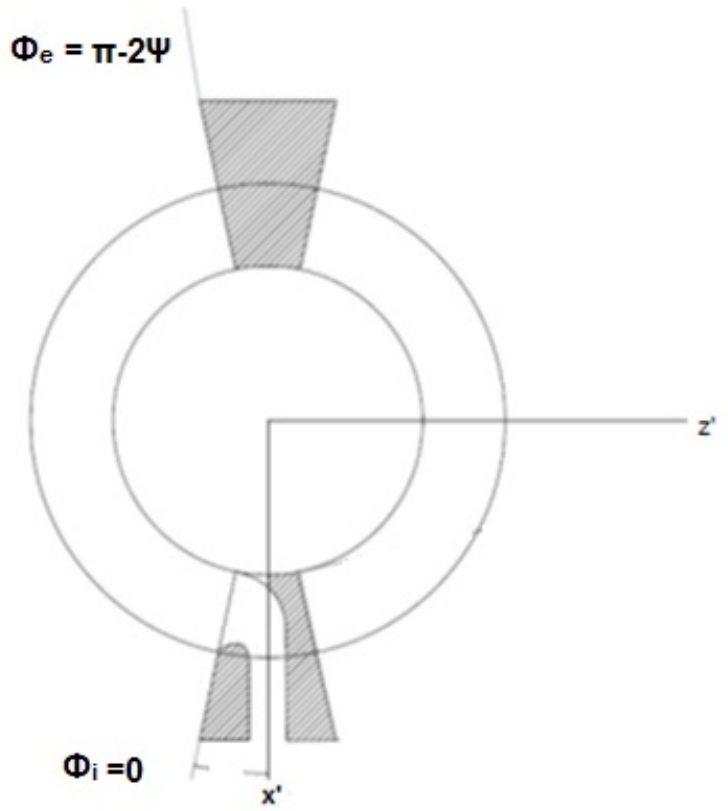

Fig. 12*:* Crank angles at which the displaced volumes are to be calculated [**Colour not necessary**].

Therefore, using a refined definition of the tip radius and hub radius in the static frame of reference, in Equations (1) to (12), an estimate of the volumetric compression ratio can be derived. A key assumption, which governs this approach, is that the position of the accumulator off-take port coincides with ϕ_e. In practice, the volumetric compression ratio can be governed by varying the location of the accumulator off-take port and the timing of the accumulator intake valve, assuming that the accumulator inlet valve is a solenoid controlled valve [15]. Alternatively, if the intake valves are simple non-return valves, then their opening and closing will be determined by the pressure in the accumulator, which would be determined by accumulator outlet valves. The volumetric compression ratio is defined as the ratio of volume in the nutating-disc compressor at the start of the compression process, to the volume in the nutating-disc compressor at the end of the compression process.

$$r_{12} = k\frac{V_{disp(\phi_i)}}{V_{disp(\phi_e)}} \tag{18}$$

2.4 Combustion and Expansion process estimation

The combustion process combines a constant-volume combustion process in the pre-chamber and a constant-pressure combustion process through a portion of the expansion chamber. The volumetric expansion ratio of the nutating disc per shaft revolution, assuming that the number of power cycles per shaft revolution is limited to two, is dictated by the crank angle at the end of the constant-pressure combustion process. Similar to the volumetric compression ratio, the volumetric expansion ratio is the ratio of the volume contained in the expander-disc chamber at the beginning of the expansion process to the volume at the end of the expansion process. Figures 13(a) and 13(b) indicate the idealized geometry of the pre-combustor.

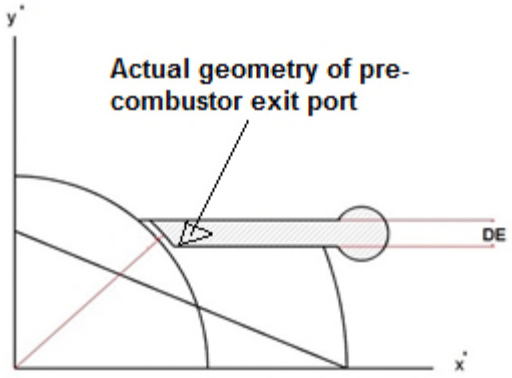

Fig. 13(a): y'-x' view of a pre-combustor [**Colour not necessary**].

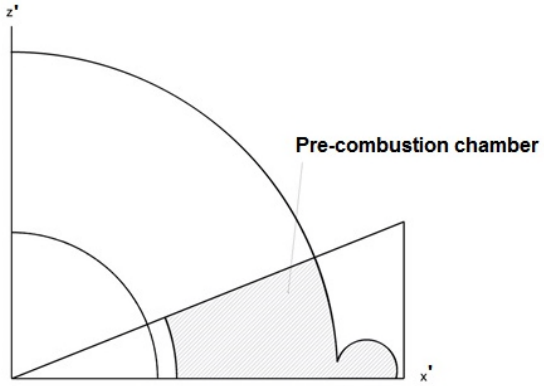

Fig. 13(b): Top-down view of half of the pre-combustion chamber [**Colour not necessary**].

In Figure 13(a), DE represents the height of the combustion chamber. The combustion chamber is positioned in such a way that it extends on one-side in the y'-direction as far as the ND-casing flat wall. In order to estimate the crank angles during the entire combustion process, it is assumed that when the combustion process starts, the nutating disc bi-conical profile completely overlays the hatched area shown in Figure 13(a) in the dynamic frame of reference. It is also assumed that the entire combustion process ceases the moment that the projected area of the nutating structure, from the dynamic frame of reference, no longer completely overlays the hatched area of combustion. This condition can be expressed mathematically by transforming r_t in the dynamic frame of reference onto the y-axis of the static frame of reference. Consequently, when this dynamic radius coincides with the minimum position of the combustor geometry, it can be mathematically assured that the projected area no longer overlays the combustor area, as expressed by Equation (19).

$$\mathrm{r_t}\sin(\alpha) - \mathrm{DE} = \mathrm{r_t}\cos(\phi)\sin(\alpha) \tag{19}$$

The crank angle, per shaft revolution, occupied during the combustion process ($\mathrm{CA_{combustion}}$) is estimated as a function of the operational speed and crank angle per shaft revolution.

$$\mathrm{CA_{combustion}} = \frac{180}{\pi}\mathrm{acos}(\phi) \tag{20}$$

Once the combustion crank angle is determined, the expansion ratio can be determined in a similar manner to that which was proposed in estimating the volumetric compression ratio. Therefore, it is possible to use Equation (16) to Equation (18) to estimate the expansion ratio. The only difference would be to specify the crank angle limits, within the derivation. The crank angle at the start of the expansion process is, $\phi_\mathrm{i} = 180^0 + CA_{combustion}$and the crank angle at the end of the expansion process is, $\phi_\mathrm{e} = 360^0$.

2.5 Auxiliary components

It is necessary to have a plenum upstream of the nutating disc array because the variations in flow into the compression chamber of the nutating disc could otherwise create significant variations in back-pressure at the exit of the upstream intermediate pressure compressor. A single toroidal plenum chamber is proposed that would connect with all the nutating disc modules. Similarly, the interface between the expander disc and the intermediate pressure turbine may require an exhaust plenum.

The following set of equations dictates the size of the inlet plenum chamber. In addition to predicting the size of the plenum chamber the following equations predict the plenum resonance frequency [19]. The volume of the toroidal plenum (V_{plenum}) is estimated as a function of the number of nutating disc cores ($\#NDs$), maximum possible length (li_{max}) of the runner manifold, actual inlet or exhaust duct length ($L_{o,duct}$), inlet and exit areas ($A_{i||plenum}$) and the speed of sound (a). Figure 14, indicates the possible arrangement of multiple nutating disc cores in the meridional view of the engine core, if the diameter of the inner nacelle constrains the number of nutating disc cores that can be circumferentially arranged around the centre line of the engine. It also indicates the maximum length of the runners and the axial length of the duct required to size the upstream plenum.

$$\cos\left[\frac{\omega li_{max}}{a}\right] = 0 \tag{21}$$

$$\left(\frac{A_{i||plenum}}{A_{e||plenum}}\right)\cot\left[\frac{\omega L_{o,duct}}{a}\right] = \frac{\omega V_{plenum}}{aA_{e||plenum}} + 2\#NDs\tan[\frac{\omega li_{max}}{a}] \quad (22)$$

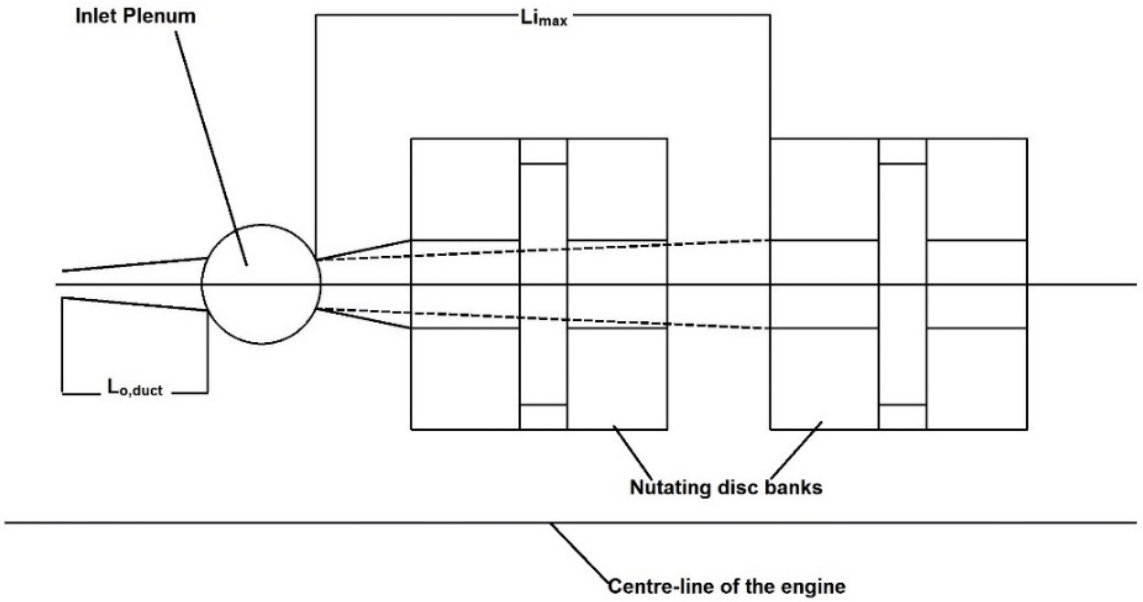

Fig. 14*:* Possible meridional view of nutating disc engine core in a geared open rotor engine, if circumferential packaging capacity is reached [**Colour not necessary**].

2.5 Engine weight and fuel burn estimation

2.5.1 Engine weight estimation

To account for the fuel-burn benefit the nutating disc engine core Y2050 geared open rotor configuration (GOR IP-drive) has over the reference Y2050 geared open rotor engine configuration, the weight of the novel components, as well at the associated turbomachinery, must be accounted for. The title of 'IP-drive' in the engine configuration designation is because the excess power produced by the nutating disc engine core in the proposed designs is transmitted to the intermediate pressure shaft.

The weight of the nutating disc core is estimated by assuming a material density and multiplying it by the volume of the parts. It is assumed the casing material used, in the Y2050 timeframe, would be gamma-titanium aluminide, given the elevated temperatures that the nutating disc core would encounter [20] and the need to avoid the 'titanium-fire' risk with conventional titanium alloys. Furthermore, the discs housed within the casing could potentially be made from ceramic matrix composites by the 2050 timeframe. To account for the weight of the casings, as a first order approximation, Lame's thick-walled cylinder formulation is used with an assumed factor of safety of 1.2 [21]. Finally, the weight of the engine's turbomachinery is estimated by employing the methods specified by Sargerser et al. [22] and Bellocq [23].

2.5.2 Fuel burn estimation

It is assumed that the reference Y2050 geared open rotor engine and the GOR IP-drive engine would be mounted on to the rear fuselage of a short-range aircraft that can carry 180 passengers 3500 NM. It is also assumed that the lift to drag ratio of the aircraft will improve and weight will be reduced, thanks to the introduction of higher-aspect-ratio carbon-fibre reinforced polymer wings, fly-by-light systems, reduced-weight cabin furnishings, hybrid laminar flow control etc. [24].

To benchmark the fuel-burn benefits that the GOR IP-drive delivers relative to the reference Y2050 geared open rotor, when installed on the same aircraft configuration and flying the same mission; non-linear fuel-burn trade-factors are applied. These trade-factors account for changes at aircraft and engine design level by resizing the aircraft and its thrust requirements to account for the change in SFC and engine weight. Figure 15 schematically represents the process to estimate the fuel

burn while taking into account the aircraft–engine 'snowballing' effect. The non-linear trade-factors used in this study were provided by Bauhaus Luftfahrt as part of the ULTIMATE project [9].

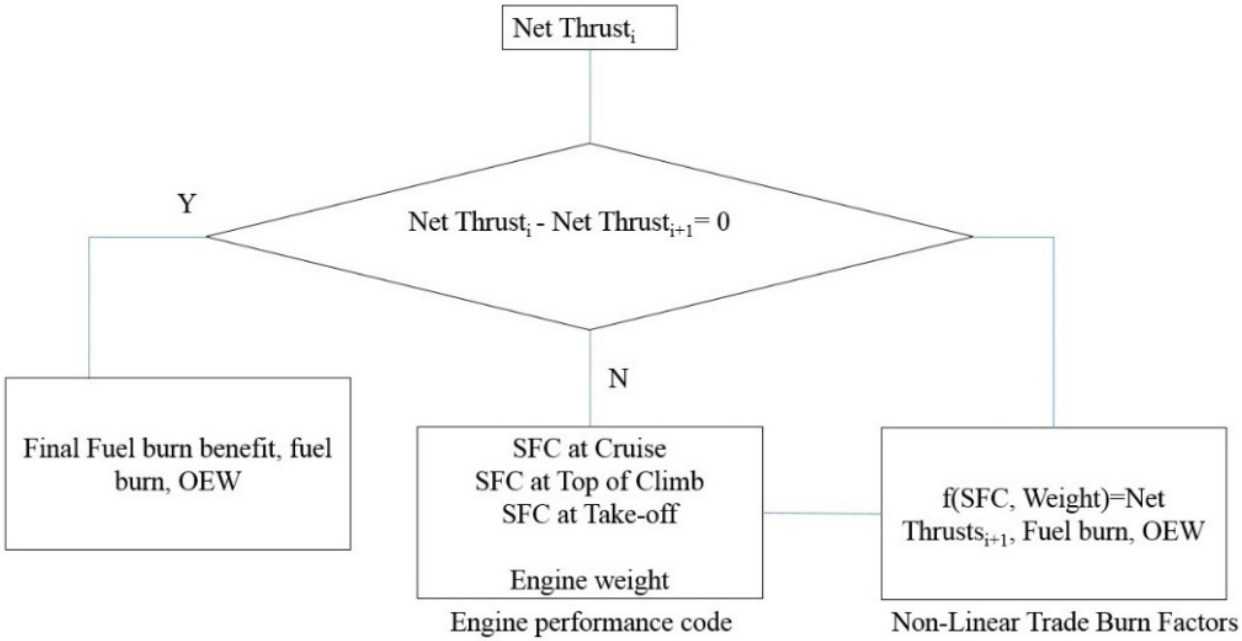

Fig. 15*:* Procedure to estimate fuel burn benefits for Y2050 short range engine concepts [**Colour not necessary**].

3 Results and Discussion

Complete validation of the proposed ND-sizing methodologies is not possible by reference to the literature, since data for the absolute validation are un-available. At this stage only a calibration of the proposed methodologies against NASA's published prototype test data is possible. This is provided in Table 2 [25].

Table 2*: Calibration of proposed ND sizing methodology*

Feature	***NASA test***	***Proposed methodology***	***Difference***
# of discs	*2*	*2*	*0%*
disc (in)	*8*	*8*	*0%*
Volumetric compression ratio (-)	*10.0*	*9.9*	*1%*
nutating angle (deg.)	*20*	*20*	*0%*
Brake horsepower (BHP)	*107*	*107*	*0%*
Total engine displacement (in^3)	*232*	*240*	*3%*

The calibration of the proposed methodology indicates that the displaced volume is over-estimated. This is most-likely because the modelled nutating disc periphery has no clearance with the casing, the walls of the wedge (within the casing) are flat as opposed to curved, and the volume occupied by the seals is not accounted for. However, an independent study performed by Nadhira et al. [26] showed a good fit with the estimate of the ND engine displacement methodology when benchmarked against a swept-volume assessment performed with CAD software.

A parametric analysis is conducted to show the influence of the compressor-disc tip radius and angle of nutation on the swept volume, at fixed hub to tip ratio. From Figure 16 it is seen that, for a fixed tip radius, as the angle of nutation increases, the swept volume increases. Similarly, for a fixed angle of nutation, the swept volume increases with an increase in compressor-disc tip radius.

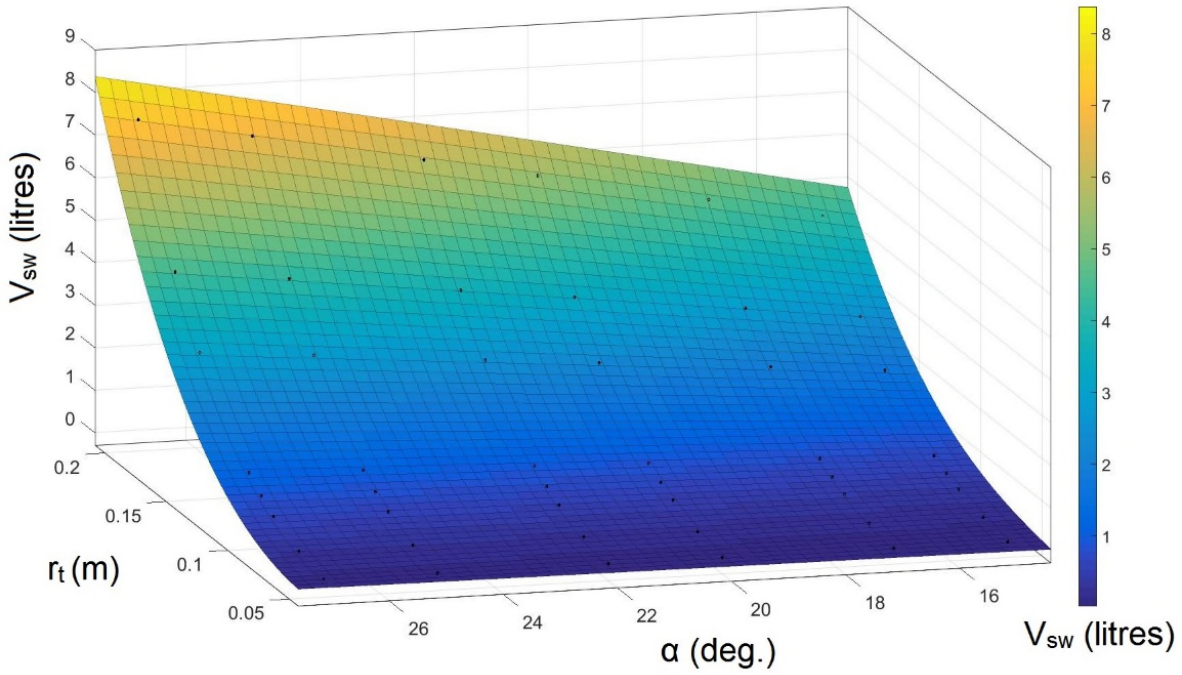

Fig. 16*:* Variation of swept volume as a function of the ND compressor tip radius and angle of nutation [**Colour necessary**].

Intuitively it would seem that, as the hub-to-tip radius ratio reduces, the swept volume of the compressor disc should increase. However, as shown in Figure 17, as the hub-to-tip ratio (HT) increases, the swept volume initially increases. This is because the inlet factor of the wedge, l_f, is fixed in the parametric study and the wedge-angle reduces as the hub to tip ratio increases. To reiterate, the inlet factor of the wedge is the radius ratio between the wedge radius and disc periphery radius.

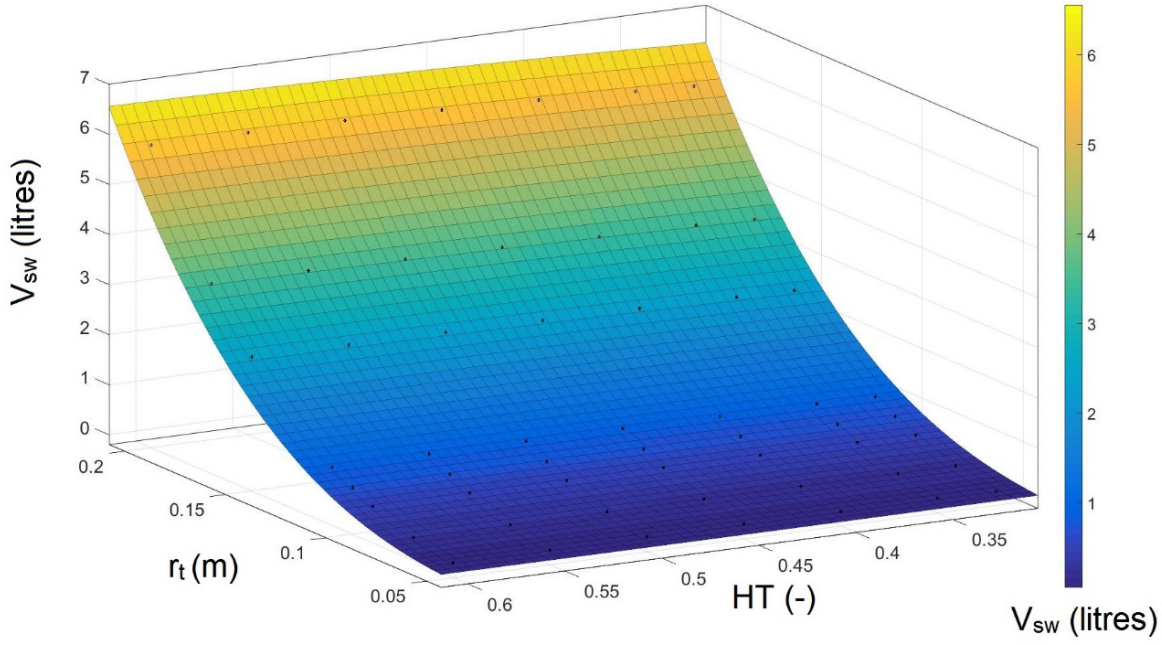

Fig. 17*:* Variation of swept volume as a function of the ND compressor tip radius and hub to tip ratio [**Colour necessary**].

The variation of the swept volume (in cubic metres) of a single nutating disc engine chamber can be expressed as a function of its tip radius (in metres), hub-to-tip radius ratio, wedge angle (in degrees) and angle of nutation (in degrees). The swept volume per compartment is estimated by employing a third order polynomial fit of the swept volume derived by using the methods highlighted from Equations (1) to (12). The presented correlation equation (23) is valid for tip radii from 0.05 m to 0.2 m and at angles of nutation from 15 degrees to 27 degrees.

$$V_{sw} = p00 + p10r_t + p01\alpha + p20r_t^2 + p11r_t\alpha + p02\alpha^2 + p30r_t^3 + p21r_t^2\alpha + p12r_t\alpha^2 + p03\alpha^3 \quad (23)$$

To account for variance in hub-to-tip radius ratios, response-surface equations for the swept volume of a single disc are presented at varying hub to tip radius ratios and wedge angles in Table 3. It is recommended to quadratically interpolate the swept volume estimate for those hub-to-tip radius ratios that are not presented.

Table 3: *Coefficients to estimate the swept volume of a single disc at varying hub-to-tip radius ratios*

HT || ψ	***p00***	***p10***	***p01***	***p20***	***p11***	***p02***	***p30***	***p21***	***p12***	***p03***
0.32 || 18.3	*1.187*	*1.476*	*0.2356*	*0.6093*	*0.3039*	*-0.00052*	*0.08306*	*0.1090*	*-0.00042*	*-0.00012*
0.35 || 17.5	*1.197*	*1.488*	*0.2332*	*0.6141*	*0.3025*	*-0.00235*	*0.83560*	*0.1088*	*-0.00235*	*0.00068*
0.40 || 16.3	*1.211*	*1.502*	*0.2360*	*0.6225*	*0.3049*	*-0.00535*	*0.08739*	*0.1098*	*-0.00462*	*-0.00028*
0.45 || 15.0	*1.227*	*1.523*	*0.2350*	*0.6276*	*0.3183*	*-0.00816*	*0.08696*	*0.1254*	*-0.00828*	*-0.00120*
0.50 || 13.7	*1.238*	*1.537*	*0.2403*	*0.6334*	*0.3252*	*-0.00713*	*0.08704*	*0.1286*	*-0.00708*	*-0.00183*
0.55 || 12.3	*1.244*	*1.544*	*0.2425*	*0.6366*	*0.3302*	*-0.00611*	*0.08749*	*0.1304*	*-0.00623*	*-0.00078*

Once the nutating disc performance and sizing methodologies are implemented within the architecture of a geared open rotor model, the performance and weight of the engine configuration can be estimated. The top of climb performance of the GOR IP-drive engine configuration is derived using the commercially available engine performance software PROOSIS and is presented in Table 4 [16]. The GOR IP-drive was found to need six nutating disc modules of the proposed disc-diameter to ensure that the flow that entered the core, from the intermediate pressure compressor, would not be choked. The expander disc was made smaller than the compressor disc to leave the downstream intermediate pressure turbine with a sensible expansion ratio and reduce the amount of power that would need to be transmitted from the nutating disc modules to the IP spool.

Table 4: *Reference top of climb performance of the GOR IP-drive engine configuration*

Parameter	***Value***	***Parameter***	***Value***
Altitude (m)	*10688*	***ND expander $f_{al,cv}$***	*0.1*
Mach no. (-)	*0.73*	***ND expander θ_1***	*0.5*
Delta ISA (K)	*10*	***ND expander θ_2***	*0.5*
W (kg/s)	*10.3*	***ND Vsw (litres)***	*1.9*
Fn (kN)	*17.0*	***ND Nmech (rpm)***	*17693*
IPC PR (-)	*6.5*	***IPT Nmech (rpm)***	*10328*
IPC η_{poly} (-)	*0.9*	***IPT PR (-)***	*2.2*
Number of ND units (-)	*6*	***IPT η_{poly} (-)***	*0.89*
ND compressor r_t (m)	*0.10*	***LPT PR (-)***	*6*
ND compressor HT (-)	*0.43*	***LPT Nmech (-)***	*6042*
ND compressor l_f (-)	*1.13*	***LPT η_{poly} (-)***	*0.88*
ND compressor α (-)	*25*	***BnBf (-)***	*15*
ND compressor r_{12} (-)	*11.2*	***BnBr (-)***	*13*
ND compressor $\eta_{s,c}$ (-)	*0.9*	***Front propeller diameter (m)***	*3.98*

Parameter	*Value*	*Parameter*	*Value*
ND expander r_t (m)	*0.09*	***Percentage clipping (%)***	*20*
ND expander HT (-)	*0.43*	***Propeller efficiency (%)***	*0.95*
ND expander α (-)	*25*	***SFC (g/kN/s)***	*10.14*
ND expander l_f (-)	*1.13*	***Combined ND weight (kg)***	*165*
ND expander $\eta_{s,e}$ (-)	*0.9*	***Engine Weight (kg)***	*3208*

Based on the presented performance values in table 4, the reference GOR IP-drive would outperform the reference GOR2050 engine configuration. However, the performance and weight estimates of the GOR IP-drive are quite sensitive to the nutating-disc-core design choices. These design variables can be grouped into SFC-dependent and engine-weight-dependent variables.

The variables that have the largest impact on the design-point SFC are the isentropic efficiency of the compressor ($\eta_{s,c}$), isentropic efficiency of the expander ($\eta_{s,c}$), the heat-loss factor through the combustion-chamber casing ($f_{ql,cy}$), the maximum temperature-change ratio during combustion (θ_1) and the average temperature-change ratio during combustion (θ_2). In practice, the compressor and expander isentropic efficiencies would be dictated by the quality of sealing, severity of turbulence generation, Reynolds number effects, and heat transfer through the casings during the compression and expansion processes. Likewise, the heat-loss factor from the combustion chambers would be dictated by the surface-area to volume ratio of the combustion chambers, the maximum firing temperature, and the effectiveness of the associated cooling systems. The maximum temperature-change ratio, in practice, will depend on the volume of the pre-combustion chamber, maximum firing temperature, shaft speed, angle of nutation and hub-to-tip radius ratio of the expander disc. The average temperature-change ratio during combustion is governed by the volumetric expansion ratio, firing frequency and the wedge angle for the expander disc.

A sensitivity study, with respect to the aforementioned variables, indicates that the isentropic compression efficiency, the heat-loss through the combustion-chamber casing walls and the average temperature-change ratio, significantly affect the design-point SFC. Figure 18 indicates the variation of the SFC-dependent nutating-disc design variables, where the reference case corresponds to Table 4. Intuitively, as the isentropic efficiencies increase and heat loss factor reduces, the SFC improves. As the maximum temperature-change ratio increases, the SFC increases because the ratio of constant-volume combustion to constant-pressure combustion decreases. However, when the average temperature-change ratio increases, the SFC decreases. This phenomenon occurs because the volumetric expansion ratio increases with an increase in the average temperature-change ratio, which in turn causes more high-grade shaft-work to be produced by the nutating disc core.

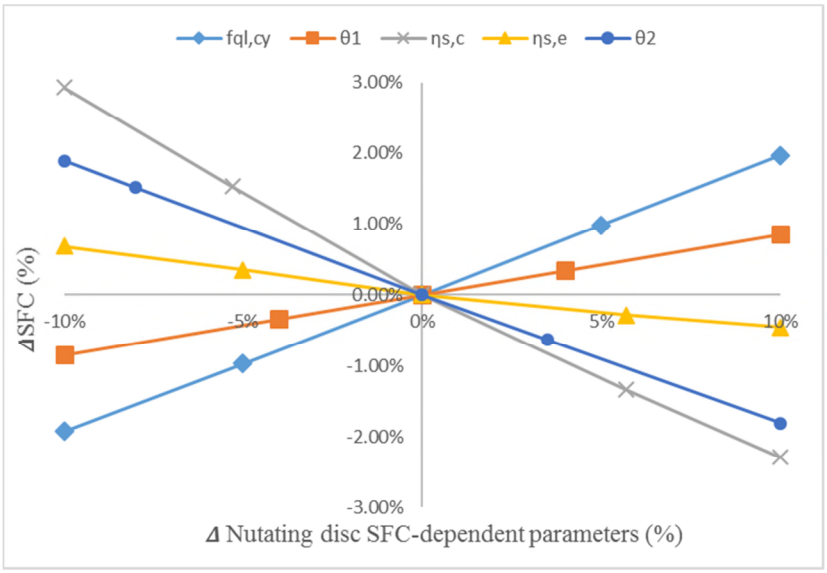

Fig. 18: *Sensitivity of the SFC dependent nutating disc design variables*[**Colour necessary**].

The nutating disc design variables that have the largest impact on the ND-core design weight are the disc tip radius (r_t), the wedge inlet factor (l_f), the hub-to-tip radius ratio (HT) and the angle of nutation (α). The sensitivity study presented in Figure 19 shows the influence these design choices have on the overall weight of the engine.

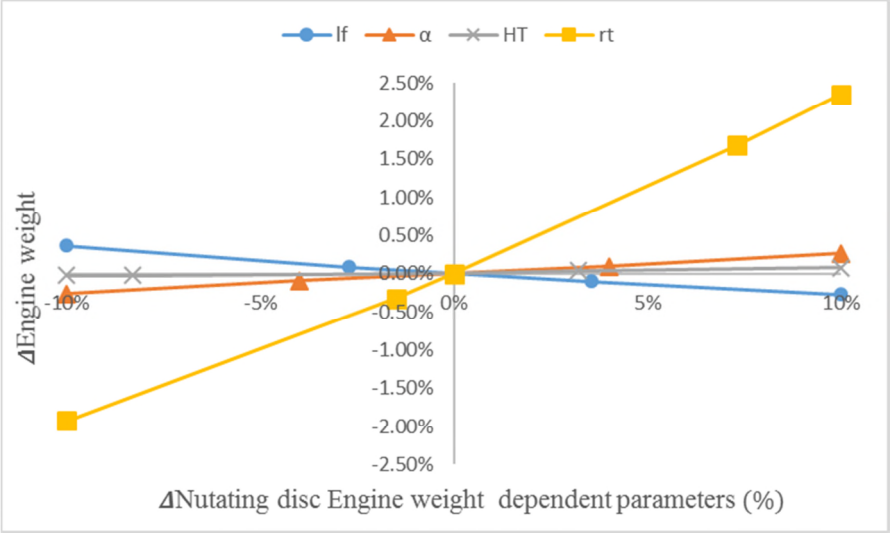

Fig. 19: *Sensitivity of the engine-weight-dependent nutating-disc design variables*[**Colour necessary**].

The sensitivity study indicates that as the tip radius, hub-to-tip radius ratio and angle of nutation increase, the weight increases. The counterintuitive trend of engine weight decrease, as the wedge inlet factor increases, corresponds to a decrease in the wedge angle for a fixed hub to tip ratio. The effect of the tip radius on weight significantly outweighs the other parameters.

To truly appreciate the severity of the choice of nutating disc design parameters, a fuel-burn analysis is conducted for the design presented in Table 4, as well as for more-optimistic and pessimistic (i.e. conservative) design assumptions. The relative-fuel-burn analysis is conducted on a representative Y2050 short-range aircraft for the mission-range of 3500 NM and uses the non-linear fuel-burn trade-factors provided by Bauhaus Luftfahrt. The results are presented in Table 5 [27].

Table 5: *Relative fuel-burn benefits for different GOR IP-drive design variants*

Parameter	***Pessimistic design***	***Reference design***	***Optimistic design***
Fn (kN)	*20.5*	*17.0*	*16.0*
ND compressor r_t (m)	*0.2*	*0.1*	*0.1*
ND compressor HT (-)	*0.32*	*0.43*	*0.50*
ND compressor l_f (-)	*1.13*	*1.13*	*1.13*
ND compressor α (-)	*27*	*25*	*17*
ND compressor r_{12} (-)	*10.8*	*11.2*	*11.0*
ND compressor $\eta_{s,c}$ (-)	*0.8*	*0.9*	*0.95*
ND expander r_t (m)	*0.2*	*0.1*	*0.1*
ND expander HT (-)	*0.32*	*0.43*	*0.5*
ND expander α (-)	*27*	*25*	*17*
ND expander l_f (-)	*1.13*	*1.13*	*1.13*
ND expander $\eta_{s,e}$ (-)	*0.8*	*0.9*	*0.95*
ND expander $f_{ql,cy}$ (-)	*0.2*	*0.1*	*0.05*
ND expander θ_1 (-)	*0.9*	*0.5*	*0.1*

Parameter	*Pessimistic design*	*Reference design*	*Optimistic design*
ND expander θ_2 (-)	*0.1*	*0.5*	*0.9*
SFC (g/kN/s)	*15.00*	*10.14*	*7.39*
Engine weight (kg)	*5191*	*3208*	*2939*
Front propeller diameter (m)	*4.18*	*3.98*	*3.92*
ND Nmech (rpm)	*2335*	*17963*	*44977*
	Off-design		
Fn at Cruise(kN)	*16.0*	*13.7*	*13.1*
Mach no.	*0.71*	*0.71*	*0.71*
Altitude (m)	*11278*	*11278*	*11278*
Delta ISA (K)	*0*	*0*	*0*
Fn at Take-off(kN)	*92.3*	*77.8*	*73.0*
Mach no.	*0.2*	*0.2*	*0.2*
Altitude (m)	*0*	*0*	*0*
Delta ISA (K)	*15*	*15*	*15*
SFC at cruise (g/kN/s)	*14.29*	*9.59*	*6.93*
SFC at Take-off (g/kN/s)	*7.38*	*4.89*	*3.52*
Fuel burn relative to GOR2050 (%)	*55.9*	*-9.4*	*-36.7*
Fuel Burn relative to Y2000 (%)	*-35.9*	*-62.8*	*-74.0*

It is apparent that the wide range of relative-fuel-burn values are highly dependent on the technology level of the SFC-dependent and weight-dependent design variables. An interesting observation is how the operating speed of each nutating disc core module scales with the degree of optimism inherent in the design. This is because the swept volume increases in the pessimistic design regime, therefore, for a fixed mass flow rate, the operational speed will decrease. The bearing life reduces as the operational speed of the nutating disc increases, thus with current state of the art bearing design the more conservative design case seems more realistic. However, by Y2050 it is assumed that advances in bearing technology would sustain the higher loads, higher temperatures and higher operational speeds that would be representative of the reference 2050 GOR IP-drive engine configuration.

When the feasibility of the engine design configuration is benchmarked against the SRIA 2050 fuel-burn-reduction target of 68%, the reference 2050 GOR IP-drive engine misses the mark, but the optimistic design meets it [24]. Figure 20 compares the relative fuel-burn benefits derived from all three 2050 GOR IP-drive design cases, the SRIA fuel burn target, and the reference GOR 2050 engine design configuration, relative to a short-range turbofan in Y2000.

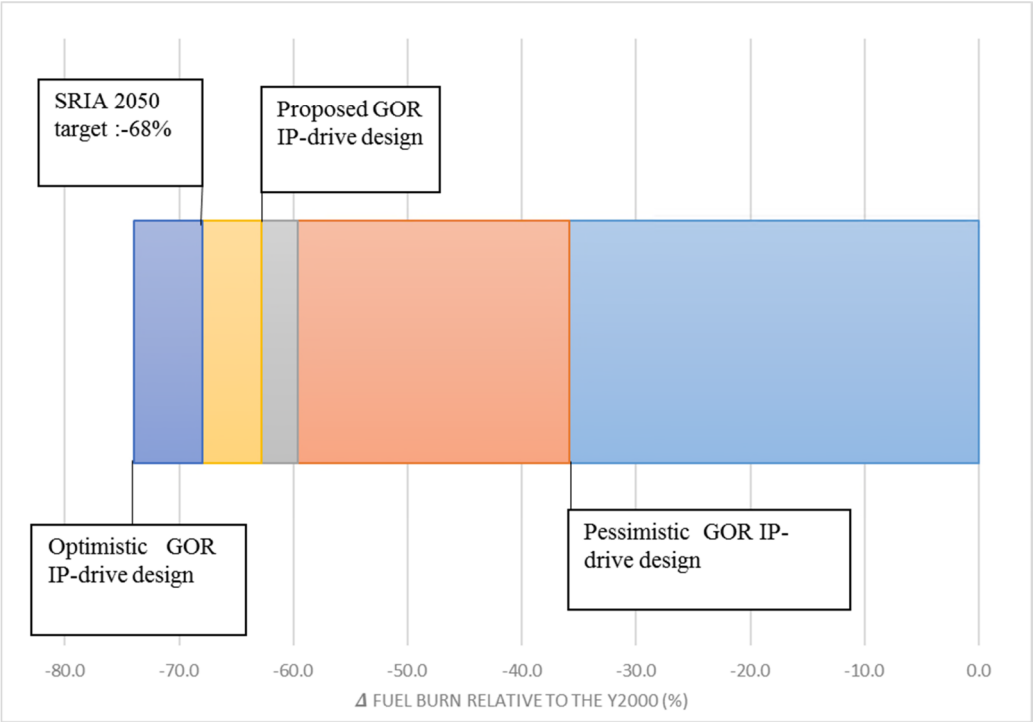

Fig. 20: *Fuel-burn targets and estimates relative to a Y2000 reference*[**Colour necessary**].

In order to meet the more-ambitious fuel-burn targets set by the optimistic 2050 GOR IP-drive, the nutating disc sealing technology needs to mature to a point where there is almost zero leakage. In addition, minimal heat loss through the casings is required. The cycle should also be more inclined towards constant-volume combustion, have minimal heat-loss from the combustion chamber and a higher volumetric expansion ratio. Improved bearing technology is also needed to sustain the higher loads and speeds seen in the optimistic design case.

5 Conclusions

A methodology is presented to account for the size of a nutating-disc engine-core module. In addition, simple correlations are presented that account for the swept volume of a nutating-disc core as a function of its tip radius, hub to tip ratio, wedge inlet factor and angle of nutation.

When the nutating-disc core is considered within the framework of a Y2050 geared open rotor engine it yields a 9.4% fuel burn reduction relative to a reference Y2050 geared open rotor. The fuel burn does not meet the SRIA Y2050 fuel-burn target, but further research providing improvements in materials and bearing technology might enable the SRIA fuel-burn target to be met.

Acknowledgement

This work has received funding from the European Union's Horizon 2020 research and innovation programme under Grant Agreement No. 633436.

Competing interest statement

This work has no explicit competing interest, as per the author's knowledge.

References

[1] Airbus, Global Market Forecast Growing Horizons 2017/2036, (2017) 1–128. http://www.airbus.com/content/dam/corporate-topics/publications/backgrounders/Airbus_Global_Market_Forecast_2017-2036_Growing_Horizons_full_book.pdf.

[2] V. Cox, N. LoBue, NextGen and the Environment, ICAO Environ. Rep. (2010) 106–108. doi:10.1017/CBO9781107415324.004.

[3] M. Darecki, C. Edelstenne, T. Enders, E. Fernandez, P. Hartman, J.-P. Herteman, M. Kerkloh, I. King, P. Ky, M. Mathieu, G. Orsi, G. Schotman, C. Smith, J.-D. Wörner, Flightpath 2050, Flightpath 2050 Eur. Vis. Aviat. (2011) 28. doi:10.2777/50266.

[4] L.L. Jensen, H. Tran, R.J. Hansman, Cruise Fuel Reduction Potential from Altitude and Speed

Optimization in Global Airline Operations *, 11th USA/Europe Air Traffic Manag. Res. Dev. Semin. (2015) 1–10.

[5] C.L. Nickol, Technologies and Concepts for Reducing the Fuel Burn of Subsonic Transport Aircraft, Nato - Otan. (2012) 1–21.

[6] C. Salpingidou, D. Tsakmakidou, Z. Vlahostergios, D. Misirlis, M. Flouros, K. Yakinthos, Analysis of turbine blade cooling effect on recuperative gas turbines cycles performance, Energy. 164 (2018) 1271–1285. doi:10.1016/j.energy.2018.08.204.

[7] D.A.B. Novelo, U. Igie, Aero engine compressor cooling by water injection - Part 1: Evaporative compressor model, Energy. 160 (2018) 1224–1235. doi:10.1016/j.energy.2018.05.170.

[8] D.A. Block Novelo, U. Igie, Aero engine compressor cooling by water injection - Part 2: Performance and emission reductions, Energy. 160 (2018) 1236–1243. doi:10.1016/j.energy.2018.05.171.

[9] T. Grönstedt, A. Rolt, N. Tantot, C. Xisto, S. Donnerhack, O. Schmitz, A. Seitz, A. Lundbladh, Ultra low emission technology innovations for mid-century Aircraftturbine engines, in: ASME Press, Seoul, 2016: pp. 1–13.

[10] A.M. Alklaibi, M.N. Khan, W.A. Khan, Thermodynamic analysis of gas turbine with air bottoming cycle, Energy. 107 (2016) 603–611. doi:10.1016/j.energy.2016.04.055.

[11] T.G. Reichel, J.-S. Schäpel, B.C. Bobusch, R. Klein, R. King, C. Oliver Paschereit, Shockless Explosion Combustion: Experimental Investigation of a New Approximate Constant Volume Combustion Process, J. Eng. Gas Turbines Power. 139 (2016) 021504. doi:10.1115/1.4034214.

[12] S.C. Gulen, Constant volume combustion the ultimate gas turbine cycle, 2013. https://www.bechtel.com/getattachment/about-us/insights/constant-volume-combustion-ultimate-gas-turbine/Constant-volume-combustion-the-ultimate-gas-turbine-cycle2013.pdf.

[13] T. Korakianitis, L. Meyer, M. Boruta, H.E. McCormick, Introduction and Performance Prediction of a Nutating-Disk Engine, J. Eng. Gas Turbines Power. 126 (2004) 294. doi:10.1115/1.1635394.

[14] T. Korakianitis, L. Meyer, M. Boruta, H.E. McCormick, Alternative Multinutating Disk Engine Configurations for Diverse Applications, J. Eng. Gas Turbines Power. 126 (2004) 482. doi:10.1115/1.1688770.

[15] T. Korakianitis, L. Meyer, M. Boruta, H.E. McCormick, One-Disk Nutating-Engine Performance for Unmanned Aerial Vehicles, J. Eng. Gas Turbines Power. 126 (2004) 475. doi:10.1115/1.1496770.

[16] PROOSIS, (2016). https://www.ecosimpro.com/.

[17] A. Alexiou, T. Tsalavoutas, TURBO 3.2 Library Reference Manual, Emoresarios Agrupados Internacional S.A., 2013.

[18] T. Gronstedt, B. Sethi, H2020-MG-2014, ULTIMATE, 2014.

[19] R.J. Pearson, W. D.E., A Rapid Synthesis Technique for Intake Manifold Design, Int. J. Veihicle Des. (1989) 659–86.

[20] J.C. Chesnutt, Titanium Aluminides for Aerospace Applications, Superalloys 1992. (1992) 381–389. doi:\url{10.7449/1992/Superalloys{\textunderscore }1992{\textunderscore }381{\textunderscore }389}.

[21] Bansal R.K, Strength of Materials, 4th ed., Laxmi Publications, Mumbai, 2010.

[22] S. D.A, L. S., Empirical expressions for estimating length and weight of axial-flow components of VTOL powerplants, NASA TM X-2406, Washington D.C, 1971.

[23] P. Bellocq, Multi-Disciplinary Preliminary Design Assessments of Pusher Counter-Rotating

Open Rotors for Civil Aviation, PhD thesis, Cranfield University, 2012.

[24] P. Heinemann, Advanced tube and wing aircraft for year 2050 timeframe, in: 55th AIAA Aerosp. Sci. Meet., Grapevine, 2017: pp. 1–50.

[25] G. Smith, W.P. Afb, M. Boruta, Meyer Nutating Disk Engine, a New Concept in Internal Combustion Engine Technology, 43rd AIAA/ASME/SAE/ASEE Jt. Propuls. Conf. Exhib. 8-11 July. (2007) 1–8. doi:10.2514/6.2007-5122.

[26] N. L., 3D URANS CFD study of a nutating disc engine compressor, MSc thesis, Cranfield University, 2017.

[27] P. Heinemann, S. Kaiser, MS2: Advanced tube and wing trade factors provided to WP1, (2016) 1–8.

Thermodynamic analysis of nutating disc engine topping cycles for aero-engine applications

Sebastiampillai, Joshua

2019-05-31

Sebastiampillai J, Rolt AM, Jacob F. (2019) Thermodynamic analysis of nutating disc engine topping cycles for aero-engine applications. Energy, Volume 182, September 2019, pp. 641-655
https://doi.org/10.1016/j.energy.2019.05.180